Journal of Applied Polymer Science

Preparation of Composite-Imprinted Alumina Membrane for Effective Separation of *p*-Hydroxybenzonic acid from Its Isomer Using Box-Behnken Design-Based Statistical Modeling

Minjia Meng,[1] Yonghai Feng,[2] Yan Liu,[1] Yun Wang,[1] Yongsheng Yan[1]
[1]School of Chemistry and Chemical Engineering, Jiangsu University, Zhenjiang 212013, China
[2]School of Material Science and Engineering, Jiangsu University, Zhenjiang 212013, China
Correspondence to: Y. Yan (E-mail: mmjybyq@aliyun.com)

ABSTRACT: Highly selective composite imprinted membrane for *p*-hydroxybenzonic acid (*p*-HB) was prepared by using semicovalent imprinting technique. A thermally reversible covalent bond was used to link *p*-HB molecule to a functional alkoxysilane monomer to generate covalently bound imprint precursor. This precursor was incorporated into a cross-linked functional silica sol with the tetraethoxysilane as cross-linker via a typical acid-catalyzed, sol-gel synthesis. Then, the SCIM was prepared through dipping and grafting on the upper side and inner pores of the Al_2O_3 microporous membrane and then removing of the template molecule after thermal treatment. Compared with composite imprinted membrane via noncovalent imprinting approach as well as the black Al_2O_3 microporous membrane, the SCIM exhibited higher membrane flux and selective rebinding of *p*-HB as well as showing excellent permeability for *p*-HB. Response surface methodology was used to investigate the best combination of separation conditions in the dynamic separation process. The optimal conditions for the separation of *p*-HB from salicylic acid were as follows: the *p*-HB concentration of 5 mg L^{-1}, the temperature of 10°C, and the flow rate of 1 mL min^{-1}. Under these conditions, the experimental selective separation factor was 32.75 ± 0.91%, which was close to the predicted selectivity coefficient value. © 2014 Wiley Periodicals, Inc. J. Appl. Polym. Sci. **2014**, *131*, 40621.

KEYWORDS: composites; functionalization of polymers; membranes; metathesis; separation techniques

Received 16 December 2013; accepted 19 February 2014
DOI: 10.1002/app.40621

INTRODUCTION

Salicylic acid (SA), also known as *ortho*-hydroxybenzoic acid or 2-hydroxybenzoic acid, was used as an analgesic as early as 400 BC, and now, it has been used in many fields including ointment, liquid, cream, or plaster, for the treatment of acne, psoriasis, warts, ichthyosis, and other hyperkeratotic disorders.[1] However, *p*-hydroxybenzonic acid (*p*-HB) as an isomer of SA, is toxic and harmful to skin at high concentration, which is usually produced along with the more desirable product SA. Therefore, it is of great necessity to develop efficient methods for the selective separation of *p*-HB from SA for ensuring the high purity of SA.

Conventional isomer separation methods, such as crystallization,[2] chromatography,[3] and microbiological[4] methods, have difficulties in the scaling-up although they could produce high selectivity. Membrane-based separation process, a newly emerging technique,[5] features many advantages over traditional separation methods, for instance, large process capability, continuous operation mode, and low-energy consumption. However, the inherent disadvantage of the membranes lies in the fact that it is difficult to retain both high selectivity and permeability.

Molecular imprinting has become a powerful method for the preparation of a cross-linked polymer matrix around an imprint molecule that is held in place, either covalently or noncovalently, by judiciously chosen functional monomers.[6] The removal of the imprint molecule yields an imprint cavity of appropriate size and chemical functionality to bind the target, thus, obtaining molecularly imprinted polymers (MIPs). MIPs have been used as sensors for detection of various compounds in selective recognition studies,[7,8] chiral separations,[9,10] as antibodies and receptors mimics,[11,12] and enzyme catalysis.[13] Recently, the challenge of involving the molecular imprinting technique in the membrane preparation process has attracted the attention of numerous researchers because it created an innovative way in molecular separations and represented a strong and cheap alternative to traditional membrane separation methods.[14–16]

The hydrogen bond-based molecular imprinting technology has been widely used for the preparation of MIPs through polymerization of

functional monomers.[17,18] For this method, excessive templates have to be used so to increase recognition cavities in the MIP matrixes. Thus, using more organic solvents to remove the templates from the MIPs often causes environmental burden.[19] In addition, due to the relative weak interaction of hydrogen bond, the thorough removal for target substances is hardly achieved.

More recently, a new semicovalent imprinting technique more efficient than the hydrogen bond-based molecular imprinting technology in the separation of isomer has been developed.[20] The imprint was covalently bound to the functional monomers through a thermally reversible carbamate bond that was formed by a direct coupling between phenol moieties on *p*-HB and isocynanate groups on (3-isocyanatopropyl) triethoxysilane (ICPTES), which is stable at room temperature and undergoes reversible cleavage at elevated temperature. It is a simple synthetic method that is highly amenable to scale up.

Inorganic ceramic membrane is an ideal support for the imprint membrane because they can be used under severe conditions, owing to their chemical and thermal stabilities, mechanical strength, and filtration performance.[21,22] In the present work, two functional silica sol was primarily prepared by taking the *p*-HB as the template molecule, ICPTES or aminopropyltriethoxysilane (APTES) as the functional monomer, and the tetraethoxysilane (TEOS) as the crosslinker. Then, Al_2O_3 ceramic membrane-based composite-imprinted membrane (CIM) for *p*-HB was prepared through coating and grafting on the upper side and inner structure of the Al_2O_3 microporous membrane by using functional silica sol and removing of the template molecule. This approach allowed simple procedures and mild reaction temperature. Another aim of this research was to investigate the effect of different interaction between template and functional monomer on the separation effect. On the basis of this work, the present study was to optimize the process for the dynamic separation of *p*-HB from its isomer (SA) using the response surface methodology (RSM), using three-level, three-variable Box–Behnken design[23] (BBD) to study the effects of the concentration, the flow rate, and the temperature on the separation effect. The performance and selective permeation mechanism of imprinted membrane were studied.

EXPERIMENTAL

Materials

Al_2O_3 microporous membranes with a nominal pore size $d_p = 2$ μm, with a thickness of 2 mm, were purchased from Hefei Great Wall Xinyuan film Technology Co., SA, *p*-hydroxybenzoic acid (*p*-HB), ICPTES, APTES, TEOS, and dimethylsulfoxide (DMSO) were all purchased from Sinopharm Chemical Reagent (Shanghai, China). All other chemicals used were of analytical grade and obtained commercially. Ultrapure water used throughout the experiments was obtained from laboratory purification system.

Synthesis of CIM

Cleaning/Hydroxylating Microporous Alumina Surfaces. The surfaces of Al_2O_3 microporous ceramic membranes were first boiled in 30% hydrogen peroxide for 30 min to introduce—OH groups on the surface for further modification. They were then boiled in deionized water for 15 min to clean the surface and dried under nitrogen condition.

Preparation of Functional Precursor. Semicovalent precursor (SP) synthesis: in a typical batch, *p*-HB (0.69 g, 5 mmol) and ICPTES (2.47 g, 10 mmol) were added to 25 mL of dry tetrahydrofuran in a round-bottomed flask and allowed to react with stirring under nitrogen at 70°C for 20 h. The solvent was removed by rotary evaporator; finally, SP was obtained after dried under vacuum condition.

Noncovalent precursor (NP) synthesis: In a typical batch, *p*-HB (0.69 g, 5 mmol) and APTES (2.21 g, 10 mmol) were added to 25 mL of anhydrous ethanol in a round-bottomed flask and allowed to react with stirring under nitrogen at 70°C for 20 h. Ethanol was removed by rotary evaporation. Then, the unreacted APTES was removed through purification of *n*-hexane. Finally, NP was obtained after dried under vacuum condition.

Preparation of Functional Silica Sol. Functionality precursor (0.8 g; SP or NP) was dissolved in 25 mL anhydrous ethanol, then 10 mL TEOS, and 15 mL deionized water were added to the mixture solution, then the pH value of solution was adjusted to 5.7 with hydrochloric acid, and then the solution was reacted at 75°C for 12 h. When the reaction was over, the solution was placed at room temperature for 24 h. Finally, functionality silica sol–based SP (SPFS) or functionality silica sol–based NP (NPFS) were obtained.

Preparation of Al_2O_3 Ceramic Membrane-Based Imprinted Membrane. The hydroxylating microporous Al_2O_3 microporous membrane was immersed into the functionality silica sol (SPFS or NPFS) at 298 K for 19 h to make the functional silica sol gelate on the upper-side and inner structure of the Al_2O_3 membrane. To make the functional silica gel film bond tightly with Al_2O_3 membrane by dehydration, the composite membrane was dried under the 50°C airtight moist steam circumstance for 15 h and then under natural condition for 24 h.

Imprint Removal. The membrane prepared with SP was immersed into DMSO in a Teflon-lined stainless steel autoclave. Several drops of distilled water were added, and then it was heated to 180°C for 4 h. The CIM-based semicovalent imprinting (SCIM), was rinsed thrice with alternately distilled water and ethanol, twice more with ethanol, and then oven dried. The possible preparation protocol of SCIM was shown in Figure 1.

The membrane prepared with NP was extracted with 100 mL mixed solvents of methanol and acetic acid (9:1, V/V) in a soxhlet apparatus for 72 h to elute the template molecular, and the elution temperature was 70°C. Finally, the CIM-based noncovalent imprinting (NCIM) was obtained by filtrating and drying.

Characterization

The precursor (SP or NP) was characterized by Infrared spectra (4000–400 cm^{-1}) recorded on a Nicolet NEXUS-470 FT-IR apparatus. The surface morphologies and cross-sectional structures of the CIM were obtained by a S-4800 scanning electron microscopy (SEM).

Membrane-Selective Binding Studies

Selective properties of imprinted membrane were evaluated performing binding tests using solutions containing *p*-HB and SA.

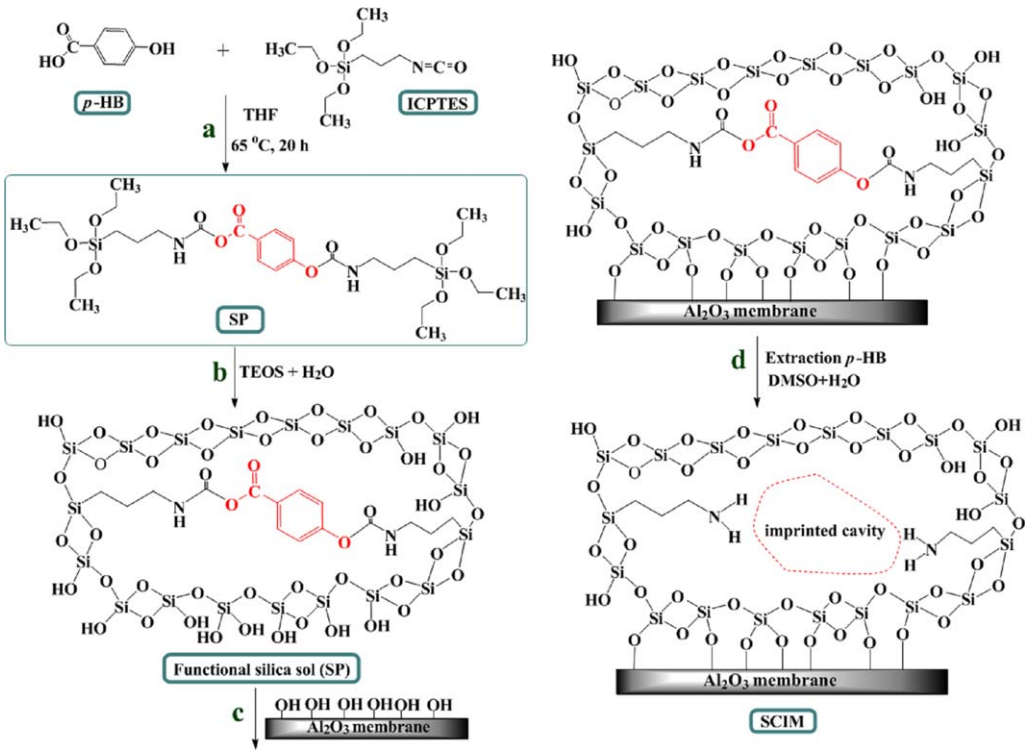

Figure 1. Schematic procedure of imprinted membrane (SCIM) preparation. [Color figure can be viewed in the online issue, which is available at wileyonlinelibrary.com.]

A piece of CIM (or a piece of blank membrane) was added into conical flask, each of which contained 20 mL solution with 100 mg L^{-1} of *p*-HB and SA, respectively. Then, it was shocked at 25°C for 12 h in a water bath oscillator. Then, substrate concentration (*p*-HB and SA) in the solution was analyzed using ultraviolet visible (UV) spectrophotometry and the binding amount of each substrate can be calculated by the following equation:

$$q_e = \frac{(C_0 - C_e)V}{W} \quad (1)$$

where C_0 (mg L^{-1}) and C_e (mg L^{-1}) represent the concentration of substrates measured at an initial and saturated binding time determined by UV spectrophotometry. V (L) and W (g) are the volume of the solution and the weight of the imprinted membrane, respectively.

The distribution coefficients (K_d), selectivity coefficients (α) of *p*-HB with respect to SA can be obtained according to eq. (2) − (3):

$$K_d = \frac{q_e}{C_e} \quad (2)$$

K_d (mL g^{-1}) represents the distribution coefficient, q_e (mg g^{-1}) and C_e (mg L^{-1}) are the equilibrium binding amount and the equilibrium concentration of the adsorbate, respectively. The selectivity coefficient α can be obtained according to the following equation:

$$\alpha = \frac{K_{d(p\text{-HB})}}{K_{dj}} \quad (3)$$

where, K_{dj} represents the distribution coefficient of competition species.

Static Permeability Experiment

Static permeation experiments were carried out using the mixture solutions containing 100 mg L^{-1} of *p*-HB and SA as the feed solution. The CIM (SCIM or NCIM) and blank membrane with an effective area of 1.5 cm^2, was fixed tightly between two chambers of a permeation cell. The volume of each chamber was 150 mL. The mixture solution of *p*-HB and SA (100 mL) of 100 mg L^{-1} in methanol was placed in the left-hand side chamber, while 100 mL methanol was placed in the right-hand side chamber. The permeation experiments were done at 25°C. Finally, the concentration of both *p*-HB and SA in the permeate solution was determined by a UV system. A separation factor (α_P) was defined as the ratio of the fluxes of *p*-HB and SA to evaluate the permeation selectivity of the membrane.

Membrane flux Experiment

The aqueous solution containing 100 mg L^{-1} *p*-HB was prepared as feed solution, and the CIM (SCIM or NCIM) and blank membrane were fitted on the ultrafiltration cell with 25 mm diameter (UF-8010, Amicon). The feed solution was permeated through the membrane (operation pressure: 0.15 MPa), and the flux of the feed solution passing the three different membranes were calculated by eq. (4):

$$F = \frac{V}{st} \quad (4)$$

where V is volume of permeate solution (mL), t and s represent operation time (min) and effective area of membrane (cm^2), respectively.

Table I. BBD Experiment Design and Result for the Optimization of the Selective Separation Factor Between *p*-HB and SA

Run	*A* (*C*: mg L^{-1})	*B* (T: °C)	*C* (*V*: mL min^{-1})	α
1	12.5	10	5	5.690
2	12.5	10	1	9.022
3	12.5	25	3	6.317
4	12.5	40	5	3.044
5	20	10	3	4.139
6	20	40	3	3.691
7	12.5	25	3	6.468
8	5	25	5	17.08
9	12.5	40	1	8.767
10	20	25	5	2.524
11	5	25	1	30.07
12	12.5	25	3	5.706
13	12.5	25	3	7.004
14	12.5	25	3	5.994
15	20	25	1	2.832
16	5	40	3	24.01
17	5	10	3	29.10

Dynamic separation of *p*-HB from SA

In the present work, a three-level, three-variable BBD was applied to determine the best separation parameters for optimizing the separation process. The concentration of *p*-HB and SA, flow rates, and temperature were input variables. The response of the experiment was the selective separation factor between *p*-HB and SA.

The selectivity factor of membrane was calculated using the following equation:

$$\alpha = \frac{q_P / C_P}{q_S / C_S} \tag{5}$$

where, q_P and q_S are the equilibrium binding amount (mg g^{-1}), C_P and C_S are the permeation concentration of the *p*-HB and SA (mg L^{-1}), respectively.

The design of real experiments is given in Table I. The behavior of the system was explained by the following quadratic (second-order) polynomial equation, which involving three significant independent variables *A*, *B*, and *C*.

$$y = \beta_0 + \beta_1 A + \beta_2 B + \beta_3 C + \beta_{11} A^2 + \beta_{22} B^2 + \beta_{33} C^2 + \beta_{12} AB + \beta_{13} AC + \beta_{23} BC \tag{6}$$

where, y is the response function, β_0 is an constant, β_1, β_2, andβ_3 are the coefficients of the linear, β_{11}, β_{22}, and β_{33} are quadratic coefficients, β_{12}, β_{13}, and β_{23} are the interaction coefficients between the three factors.

The regression coefficients of individual linear, quadratic, and interaction terms could be used to estimate the response. A total of 17 experiments were needed to estimate the full model. All the experimental data were statistically analyzed by the software package Design-Expert 8.0.5b. *P*-values of less than 0.05 were considered to be statistically significant.

RESULTS AND DISCUSSION

Characterization

To ascertain the successful preparation of functional precursor, FT-IR spectra (Figure 2) were obtained for ICPTES, SP, APTES, and NP. From Figure 2(a), the strong adsorption band around 2272 cm^{-1} could be ascribed to —N=C=O band of ICPTES. When compared with ICPTES, the immediate disappearance of the adsorption band around 2272 cm^{-1} and the observed features around 3317 cm^{-1} resulted from N—H stretching vibrations both indicated the successful preparation of SP.

From Figure 2(b), for APTES, the bands around 2927 cm^{-1} resulted from C—H vibrations. A characteristic feature of NP compared with APTES was Ar—H band around 857 and 790 cm^{-1}, which suggested the reaction between APTES and *p*-HB. Compared with APTES, the wide and strong adsorption band between 2500 and 3500 cm^{-1} in NP indicated the hydrogen bond may form between APTES and *p*-HB.

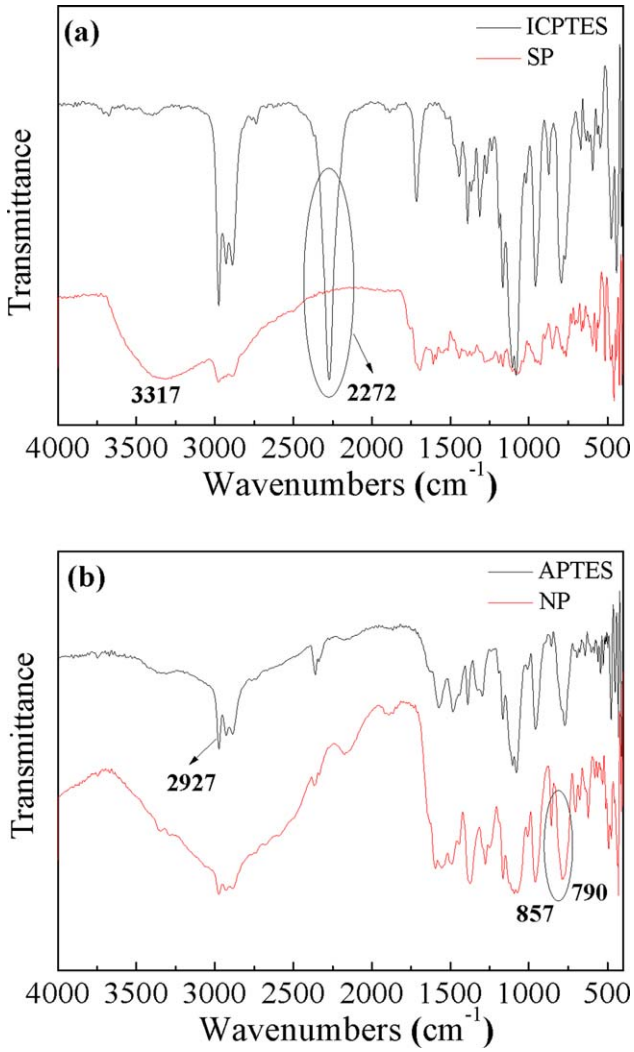

Figure 2. FT-IR spectra of ICPTES and SP (a), APTES and NP (b). [Color figure can be viewed in the online issue, which is available at wileyonlinelibrary.com.]

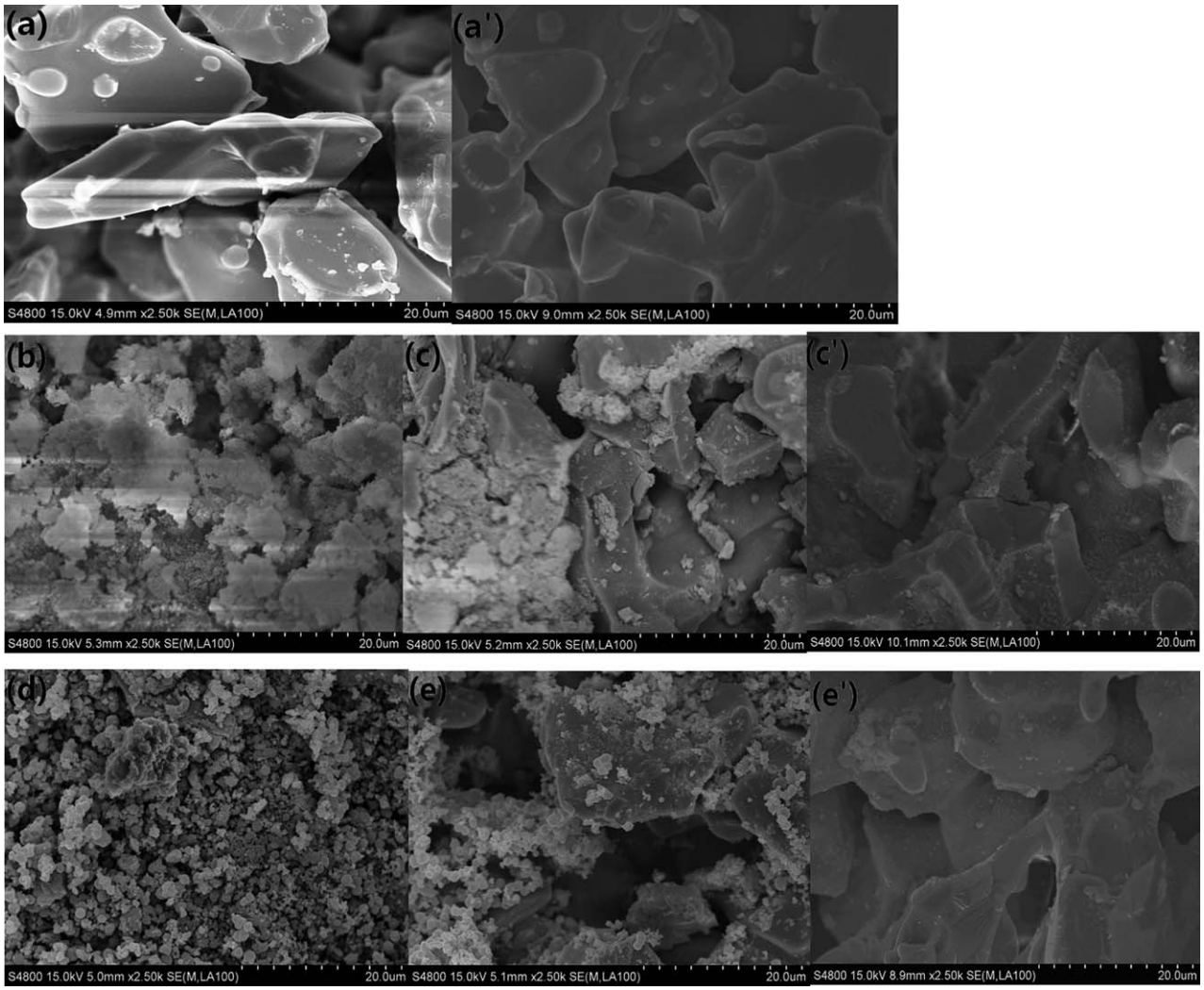

Figure 3. SEM images of surface of (a) Al_2O_3 ceramic membrane, (b) SCIM (before elution), (c) SCIM (after elution), (d) NCIM (before elution), and (e) NCIM (after elution). SEM images of cross-section of (a′) Al_2O_3 ceramic membrane, (c′) SCIM (after elution), and (e′) NCIM (after elution).

The microscopic structures of surface and cross-section of the prepared CIM were studied by using SEM with gold-sputtered samples. The morphologies of surface and cross-section of SCIM and NCIM (before elution and after elution) were exemplified by the SEM in Figure 3. Compared with the Al_2O_3 ceramic membrane, the surface of SCIM and NCIM were roughly, meaning that both of them were covered by a thick imprinted layer after the polymerization procedure, shown in Figure 3(b,d). From the cross-section morphology of Al_2O_3 ceramic membrane, SCIM and NCIM, the SEM pictures [Figure 3(a′,c′,e′)] showed there were great difference between the morphology of Al_2O_3 ceramic membrane and imprinted membrane (SCIM and NCIM). The Al_2O_3 ceramic membrane displayed a smooth cross section, whereas the cross sections of SCIM and NCIM [Figure 3(c′,e′)] were covered by a thin imprinted layer in the inner pores of Al_2O_3 ceramic membrane after imprinting polymerization. The results suggested that the sol-gel–imprinted polymer was coated not only on the outer surface but also in the inner pores of the Al_2O_3 ceramic membrane. After elution, nongrafted polymer, residual initiator and the template *p*-HB blocking the pores of the surface and inner of the CIM were removed from the imprinted membrane. The formation of irregular pores is observed again from the surface morphology of imprinted membrane, shown in Figure 3(c,e).

Membrane Flux Studies

The relationship between operation time and flux of *p*-HB aqueous solution was recorded in Figure 4. Compared with the flux of Al_2O_3 ceramic membrane, SCIM and NCIM are high at the beginning but decline later. With the increase of operation time, the imprinted membranes are impacted gradually and some of the inner pores may be jammed, thus the flux of membranes sharply declines. It was also observed that the water flux of *p*-HB aqueous solution was in an order of Al_2O_3 ceramic membrane < NCIM < SCIM. It indicated that the imprinted polymer coating had a limited effect on the physical structure of the membrane. The higher water flux of SCIM and NCIM was probably due to lots of selective cavities on the outer surface and inner pores in the Al_2O_3 ceramic membrane, which were beneficial to the accessibility of recognition sites and mass

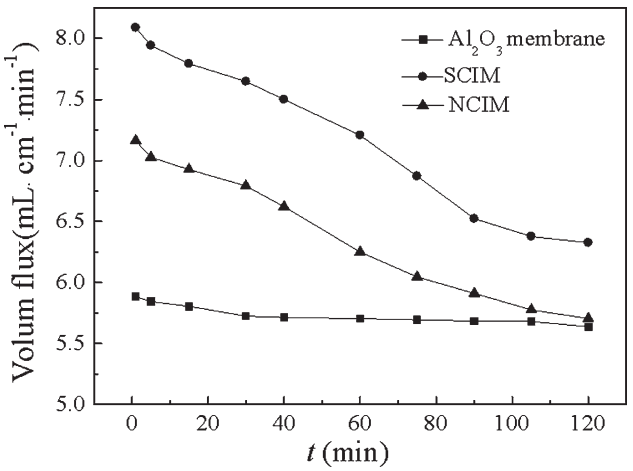

Figure 4. The flux of the Al_2O_3 ceramic membrane, SCIM, and NCIM.

transport for *p*-HB. However, the permeation flux through SCIM slightly higher than that of NCIM indicated that semicovalent imprinting technique more significantly facilitated the transport of *p*-HB for the imprinted membrane than NCIM technique.

Membrane Selectivity Studies

Batch Binary Adsorption Studies of Membrane. To study the effects of imprinting approach on the selective adsorption behavior of imprinted membranes, two types of molecularly imprinted membrane, SCIM and NCIM were synthesized in this work. The binary adsorption experiment is an important investigation used to image the selectivity of the imprinted membrane. The binary adsorption experiments for the coexisting compound (*p*-HB and SA) on different membranes were carried out at the concentration of 100 mg L^{-1}. The rebinding capacities of the Al_2O_3 ceramic membrane, SCIM, non-SCIM, and NCIM for *p*-HB and SA are shown in Figure 5. Compared with the capacities of the SCIM and the Al_2O_3 ceramic membrane, the capacities of the non-SCIM toward SA and *p*-HB were similar, which were higher than those of the Al_2O_3 ceramic membrane but much lower than those of the SCIM, especially for *p*-HB. It indicated that the nonspecific adsorption of both SA and *p*-HB for non-SCIM, while more specific binding sites were probably exposed on the surface and inner pores of SCIM than that of non-SCIM, which made the adsorption capacity of SCIM much stronger.

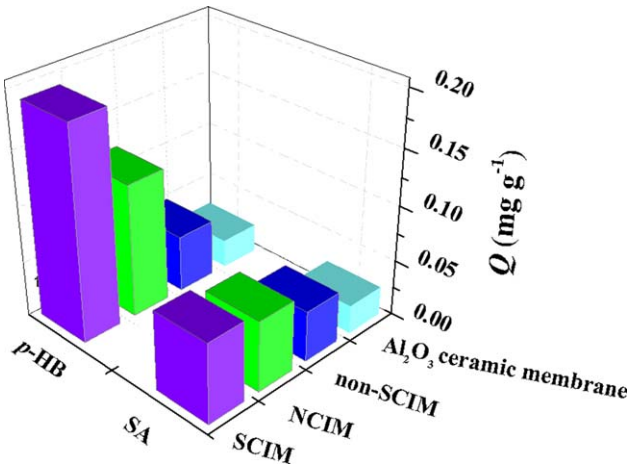

Figure 5. Binary adsorption of *p*-HB and SA by Al_2O_3 ceramic membrane, SCIM, non-SCIM, and NCIM. [Color figure can be viewed in the online issue, which is available at wileyonlinelibrary.com.]

As seen in the figure, compared with Al_2O_3 ceramic membrane, both SCIM and NCIM exhibited higher adsorption capacity for *p*-HB than SA, indicating higher rebinding selectivity for *p*-HB, which was attributed to more affinity binding sites on the surface of imprinted membrane. However, the adsorption amount of *p*-HB onto SCIM was apparently higher than that of NCIM, while the uptake of SA onto SCIM and NCIM was nearly the same. The results implied that it was much easier for *p*-HB to access SCIM than NCIM due to the stronger driving force obtained from semicovalent imprinting process.

Table II presented the K_d and α values of the Al_2O_3 ceramic membrane, SCIM, non-SCIM, and NCIM. The α values of SCIM and NCIM for *p*-HB relative to SA were 3.120 and 2.086, respectively, higher than the corresponding α of non-SCIM(0.9011) and Al_2O_3 ceramic membrane (1.002), indicating that the imprinted membrane had higher adsorption selectivity than that of either the nonimprinted membrane or black Al_2O_3 ceramic membrane. In addition, α value of SCIM was higher than that of NCIM, demonstrating the semicovalent imprinting approach more effective than NCIM technology in the separation of *p*-HB and SA.

Perm-Selectivity of Imprinted Membranes. To further evaluate the effect of imprinted membranes prepared with different imprinting approaches on the permeability performances, competitive permeation experiments were carried out for *p*-HB verses SA. The permeation concentration of *p*-HB and SA through the Al_2O_3 membrane, SCIM and NCIM were performed at the feed mixture concentration of 100 mg L^{-1} in 3 h. The permeation amount of *p*-HB and SA through different membranes depending on time was shown in Figure 6. According to the time-dependent permeation curves on the Al_2O_3 membrane, the amount of *p*-HB and SA in the receiving chamber were nearly the same, indicating that the imprinted membranes did not generate specific penetrating path for *p*-HB to pass. However, the amount of *p*-HB on SCIM and NCIM were higher than that of SA, showing that specific penetrating path for *p*-HB was generated on the imprinting membranes. It is obviously seen that the transport rate of *p*-HB for SCIM was much faster than that of NCIM and the amount of *p*-HB in the receiving chamber much higher than that of NCIM. It demonstrated that the imprinting approach significantly affected the transport rate of *p*-HB for the imprinted membrane.

From Table III, the values of imprinting factor α_p of Al_2O_3 membrane, SCIM, and NCIM were 1.198, 5.390, and 3.100, respectively. The data indicated that the imprinting process enhanced the perm-selectivity of the membrane. The SCIM having a higher separation factor than the NCIM suggested noncovalent molecular imprinting approach was deemed unsuccessful, presumably because of the lack of strong intermolecular interactions that can be established between the *p*-HB and the

Table II. Parameters of Batch Adsorption Selectivity of *p*-HB and SA

	p-HB			SA	
	$q_{p\text{-HB}}$ (mg g^{-1}) × 10^{-3}	$K_{dp\text{-HB}}$ (L g^{-1}) × 10^{-3}	α	q_{SA} (mg g^{-1}) × 10^{-3}	K_{dSA} (L g^{-1}) × 10^{-3}
Al_2O_3 membrane	25.09	0.24623	1.002	25.33	0.2459
NCIM	120.6	1.347	2.086	63.34	0.6455
SCIM	192.0	2.354	3.120	71.70	0.7356
non-SCIM	44.71	0.4652	0.9011	49.86	0.5163

functional monomer. The semicovalent imprinting strategy was used by generating a sacrificial spacer through the reaction of ICPTES with *p*-HB. After formation of the sol-gel, the bonds linking the template to the matrix were cleaved and generated a pocket of the appropriate size bordered by amine groups that could aid in the recognition of *p*-HB through weak hydrogen-bonding interactions. This means that membrane prepared by semicovalent imprinting approach was more beneficial for the separation of *p*-HB and SA.

Selective Permeation Mechanism

Two major mechanisms applied in analyzing the selective transport can be regarded: (i) facilitated permeation driven by preferential sorption of the template due to affinity binding–slower transport of other solutes and (ii) retarded permeation due to affinity binding–faster transport of other solutes, until a saturation of imprinted sites with template is reached.[24] The aforementioned permeability experiments showed that the imprinted membranes showed higher diffusion rate for the template molecule (*p*-HB) than for the completing molecule (SA). The acquirement of this property depends on the specific binding sites which existed in the outer surface and inner pore of the membrane. It could be confirmed by the SEM images of surface and cross section of imprinted membranes. The transport of *p*-HB across the membrane occur via a fixed carrier-mediated (facilitated) process by adsorbing on and desorbing from the imprinted layer on the composite membrane.

According to the principle of molecular imprinting, the imprinted membrane prepared by noncovalent or semicovalent approach existed a great number of imprinted sites in the CIM for specific rebinding with the template. So the separation process of CIM may be speculated as follows: template molecules (*p*-HB) can freely diffuse in the feed solution. When *p*-HB diffuse to the membrane surface, they preferentially react with the functional groups inside the CIM, forming complexes through interaction (hydrogen bond, electrostatic interaction, etc). This is because the size and the cavities inside the CIM matched the template molecules well. In addition, the gradients of concentration cause *p*-HB and functional groups to dissociate by destroying bonds between them. Then *p*-HB can combine with other functional groups nearby. In this way, template molecules were transported from one chemical binding site to another until they reached the permeate side of the CIM. It can be also concluded that different selective separation of *p*-HB and SA was due to the different strength of the binding interaction between templates and membranes. Therefore, such transport mechanism for permeation of the *p*-HB and SA toward SCIM or NCIM was accordance with the facilitated mechanism mentioned above, which is illustrated in Scheme 1. It was believed that the transport-selectivity mechanism was a good indication for practical application of this kind of imprinted membrane in continuous separation rather than only adsorbent for batch adsorption.

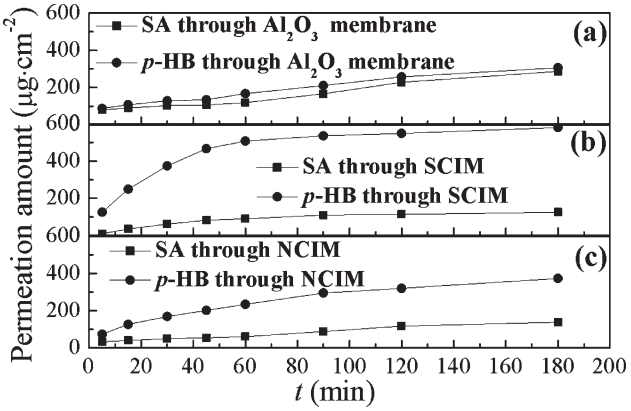

Figure 6. Time-permeation curves of *p*-HB and SA through the Al_2O_3 membrane, SCIM, and NCIM (Feed ion concentration = 100 mg L^{-1}).

Design of RSM for Optimization of Dynamic Separation

For industrial application, a dynamic separation study is essential for continuous-flow systems. The optimization step of proposed method was carried out using a BBD. SCIM was selected to study the dynamic separation of *p*-HB and SA. Several variables that could potentially affect the selective separation effect were chosen such as: the concentration of *p*-HB (mg L^{-1}), the temperature (°C), and the flow rates (mL min^{-1}).

Statistical Analysis and the Model Fitting. To study the combined effect of independent variables (separation concentration,

Table III. Average Flux and Separation Factor for the Al_2O_3 Membrane, SCIM, and NCIM (Operation Time = 3 h)

	Average flux (μg cm^{-2})		
Membrane	SA	*p*-HB	α_p
Al_2O_3 membrane	146.3	175.4	1.198
SCIM	78.48	423.0	5.390
NCIM	72.36	224.3	3.100

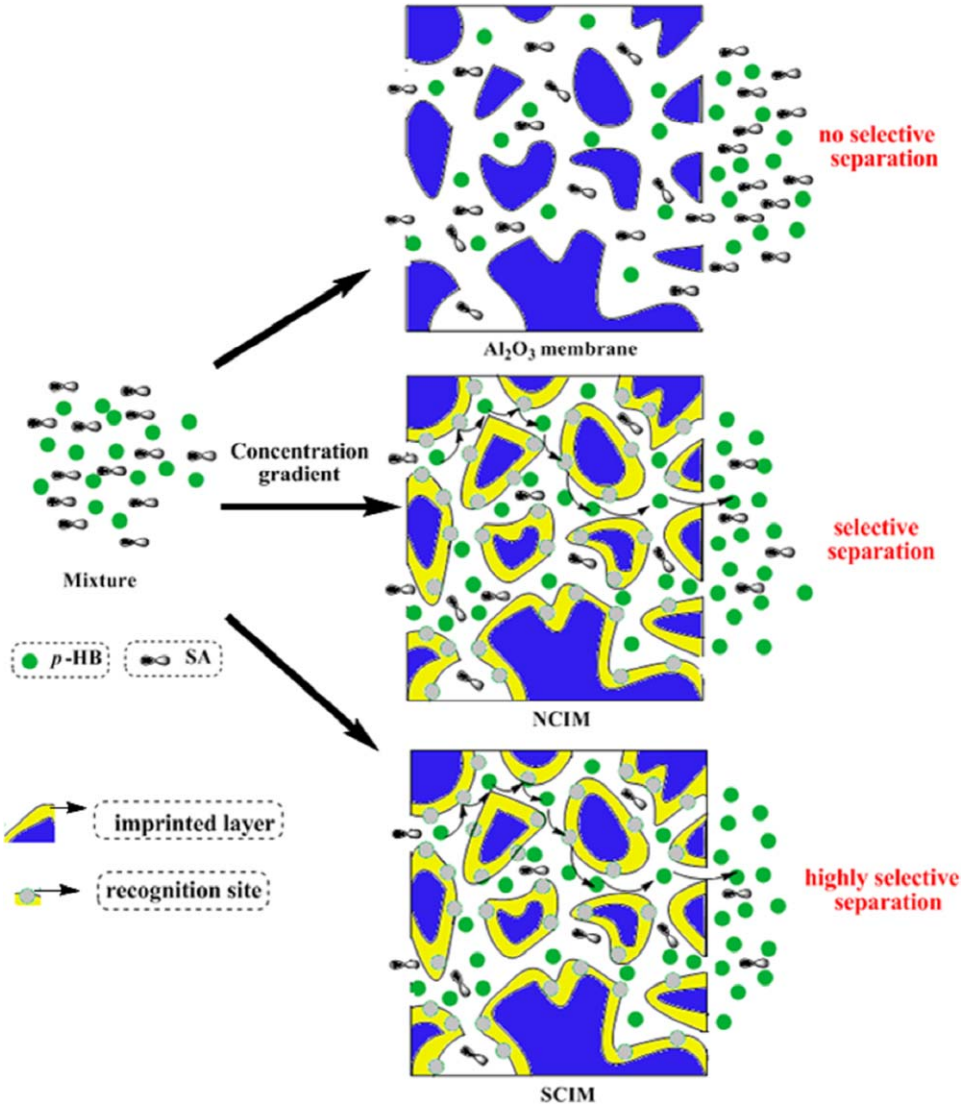

Scheme 1. Scheme of selective transport mechanism for permeation of the p-HB and SA towards the Al_2O_3 membrane, SCIM and NCIM. [Color figure can be viewed in the online issue, which is available at wileyonlinelibrary.com.]

flow rate, and temperature) on the separation effect, there were a total of 17 runs with different combinations of the physical parameters for optimizing the three individual parameters in the BBD. The selective separation factors of *p*-HB and SA according to the factorial design are shown in Table I.

Results showed that the selective separation fact ranged from 2.524 to 30.07. This design permits the response to be modeled by a second-order polynomial equation that allows estimation of the main, quadratic, and interactive effects of the factors on the separation effect under study.[25] The values of regression coefficients were calculated, the response variable and the test variables are related by the following second-order polynomial equation:

$$y=6.30+10.89A-1.05B-2.79C+7.72A^2 +1.22B^2-0.89C^2+1.16AB+3.17AC-0.60BC \quad (7)$$

Significant terms in the model for the response were found by analysis of variance (ANOVA) and significance of the regression model was checked by *F*-test and *P*-value shown in the Table IV. The ANOVA of regression model demonstrates that the model is significant with low probability ($P<0.0001$). The goodness of fit of the model can be checked by the determination coefficient (R^2). The value of adjusted R^2 (0.9904) indicated that only 0.96% of the total variations were not explained by this model. Plus, the value of determination coefficient ($R^2=0.9958$) indicates good relation between the experimental and predicted values of the response.

The lack of fit measures the failure of the model to represent data in the experimental domain at points which are not included in the regression. The nonsignificant value of lack of fit (>0.05) revealed that the quadratic model is statistically significant for the response. The *P*-value was also used as a tool to check the significance of each coefficient, and the smaller the *P*-value was, the more significant the corresponding parameters in the regression mode were. The ANOVA of the regression model showed, which the quadratic model was significant, as

Table IV. Estimated Regression Model of Relationship Between Response Variables (α) and Independent Variables (*A*, *B*, and *C*)

Factor	SS	*df*	MS	*F*	*P*	
Model	1329.02	9	147.67	184.64	<0.0001	Significant
A	948.04	1	948.04	1185.40	<0.0001	
B	8.90	1	8.90	11.13	0.0125	
C	62.45	1	62.45	78.09	<0.0001	
AB	5.38	1	5.38	6.73	0.0357	
AC	40.20	1	40.20	50.27	0.0002	
BC	1.43	1	1.43	1.79	0.2231	
A^2	250.81	1	250.81	313.60	<0.0001	
B^2	6.26	1	6.26	7.82	0.0266	
C^2	3.31	1	3.31	4.13	0.0816	
Lack of fit	4.63	3	1.54	6.36	0.0530	Not significant

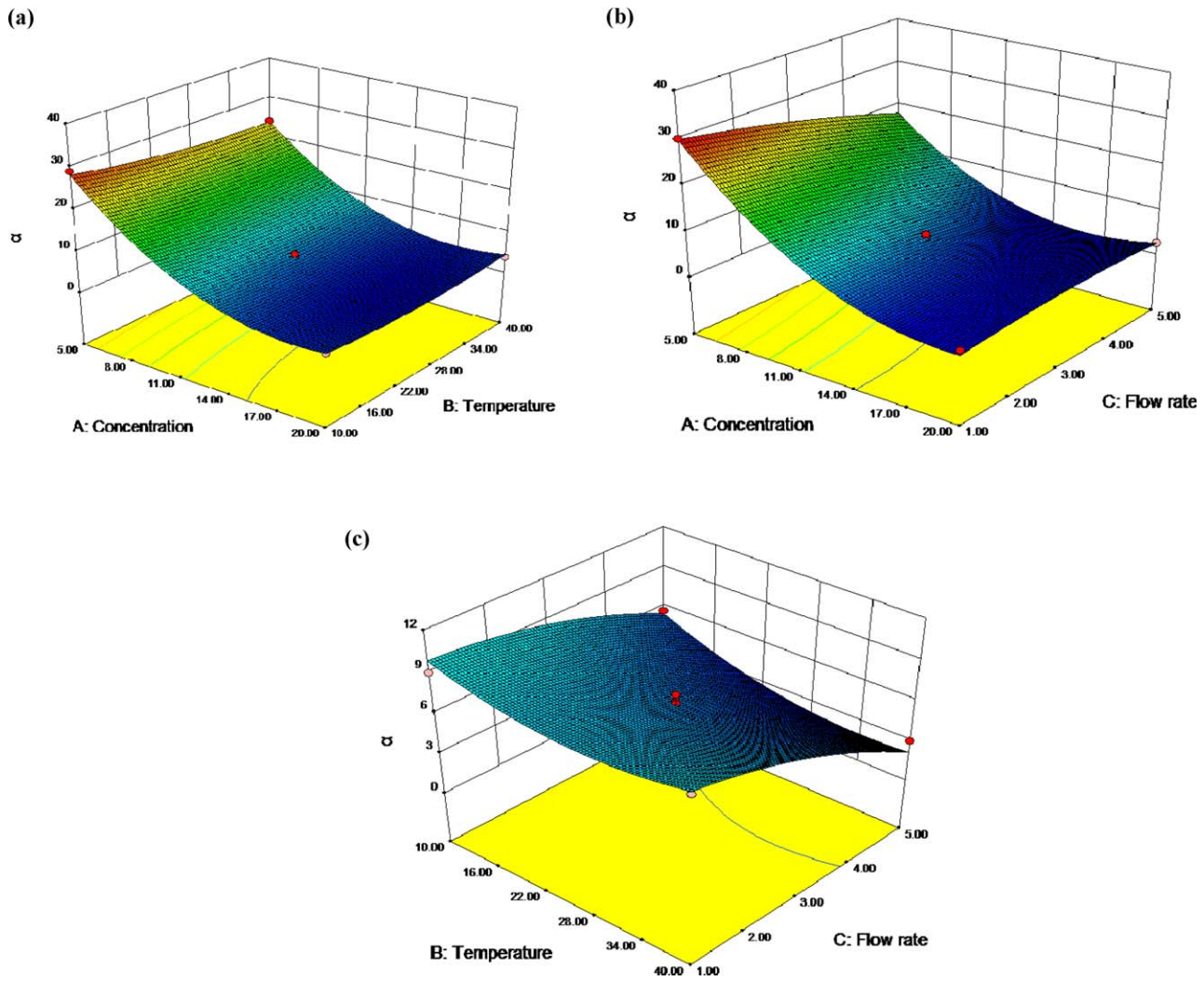

Figure 7. Response surfaces plots for selectivity coefficients as a function of (a) concentration of *p*-HB and temperature, (b) concentration of *p*-HB and flow rate, and (c) flow rate and temperature. [Color figure can be viewed in the online issue, which is available at wileyonlinelibrary.com.]

was evident from the *F*-test (F model = 184.64) with a very low probability value ($P < 0.0001$).

The contribution of each parameter/factor (first and second order) besides the interaction between them on the separation effect was shown in Table IV. All coefficients with *P*-values less than 0.05 are significant. As seen in Table IV, the analyses indicated that *A*, *B*, *C*, *AB*, *AC*, A^2, B^2 are significant model terms for separation of *p*-HB from SA, while the other term coefficients (*BC*, C^2) were not significant ($P > 0.05$).

Three-Dimentional Response Surfaces. Commonly, three-dimensional (3D) response surface were plotted as a function of two factors, maintaining all other factors at fixed levels helpful in understanding both the main and their interaction effects of these two factors. In this work, to study the effect of parameters and their interactions on the separation effect, as well as to calculate the optimum separation factor, 3D response surface plots for the measured responses were formed based on the model equation [eq. (7)]. As the regression model has three independent variables, one variable was held at constant at the central level for each plot, thus, a total three response 3D plots were produced for responses. The results of selective factor between *p*-HB and SA affected by the concentration, flow rate, and temperature are presented in Figure 7. It shows the 3D response surfaces as the functions of two variables at the centre level of other variables, respectively.

In Figure 7(a), when the 3D response surface plot were developed for the selective separation of *p*-HB from SA with varying *p*-HB concentration in the mixture (*p*-HB and SA) solution and temperature at fixed flow rate 3 mL min^{-1}. It indicated that the selective separation factor was mainly affected by the varied *p*-HB concentration. The *a* value rapidly increased with the decrease in the *p*-HB concentration from 20 to 5 mg L^{-1} and slightly increased with the decrease in the temperature from 40 to 10°C. Therefore, the effect on the separation of *p*-HB from SA was favored at the low *p*-HB concentration and relative low temperature. It might be for the reason that the more feeding of adsorbate on per unit surface area of the membrane caused the faster saturation of the molecularly imprinted membrane, which will affect the separation effect. So imprinted membrane can be predicted to be exploited in purification of trace analytes in the complex matrix. The high temperature decreased the separation effect, showing that less SA molecules were required to satisfy the maximum adsorption capacity of imprinted membrane. Therefore, the adsorption of SA on imprinted membrane was favored at low temperature, indicating an exothermic process.

Figure 7(b) giving the selective separation of *p*-HB from SA as a function of concentration and flow rate at fixed temperature (25°C), indicated that the selective separation factor significantly increased with the decrease in the concentration of *p*-HB in SA from 20 to 5 mg L^{-1} and slightly increased with the decrease of the flow rate from 5 to 1 mL min^{-1}. The effect of the lower flow rate on the selective effect was due to an increase in the residence time, which will have enough time to diffuse into the binding sites on the imprinted membrane and they passed the membrane fast before equilibrium occurred.

Figure 7(c) shows the 3D response surface plot at varying temperature and flow rate at fixed SA concentration of 12.5 mg L^{-1}. It indicated that the maximum *a* value can be achieved when temperature and flow rate at 10°C and 1 mL min^{-1}, respectively.

Optimization and Verification of the Model. From Figures 7(a–c), it can be concluded that the optimal conditions giving the maximum response for selectivity coefficient (32.81) was found in conditions of $A = 5$ mg L^{-1}, $B = 10$°C, $C = 1$ mL min^{-1}.

For their validation of the optimum conditions, triplicate confirmatory experiments were carried out under the optimized conditions and the average separation factor (*a*) was $32.75 \pm 0.91\%$. The results are closely related with the data obtained from optimization analysis, indicating BBD could be effectively used to optimize the separation *p*-HB from SA.

CONCLUSIONS

Highly efficient CIMs (SCIM) with artificially introduced affinity to *p*-HB was prepared based on Al_2O_3 ceramic membrane using a thermally reversible semicovalent imprinting strategy. Compared with NCIM, SCIM exhibited higher membrane flux and higher selective rebinding of *p*-HB, as well as showing excellent permeability for *p*-HB. SCIM was found to be the promising imprinted membrane to increase the effect on separating *p*-HB from SA. RSM was used to estimate and optimize the experimental variables in the dynamic separation process: the concentration of *p*-HB (mg L^{-1}), the temperature (°C), and the flow rate (mL min^{-1}). This study showed that RSM was a suitable technique to optimise the best conditions for obtained maximum separation factor. Under the optimal conditions of *p*-HB concentration at 5 mg L^{-1}, temperature at 10°C, flow rate at 1 mL min^{-1}, the experimental selectivity factor was $32.75 \pm 0.91\%$, which was close to the predicted selectivity factor value. All the aforementioned indicates the potential application of the imprinted membranes for highly selective separation of analogues. Further, it is useful and practical in purification of trace analytes in the complex matrix.

ACKNOWLEDGMENTS

This work was financially supported by the National Natural Science Foundation of China (Nos. 21107037, 21176107, 21174057, 2100403, 21207051), National key basic research development program (973 Program, No. 2012CBB21500), Ph.D. Programs Foundation of Ministry of Education of China (Nos. 20123227120015, 20110205110014) and Natural Science Foundation of Jiangsu Province (BK2011461, SBK2011459, BK2011514). China Postdoctoral Science Foundation funded project (No. 2013M530240). Ph.D. Innovation Programs Foundation of Jiangsu Province (No. CXZZ13_0680).

REFERENCES

1. Tsai, J. C.; Chuang, S. A.; Hsu, M. Y.; Sheu, H. M. *Int. J. Pharm.* **1999**, *188*, 145.
2. Lamberti, G. *Eur. Polym. J.* **2011**, *47*, 1097.

3. He, M.; Du, W.; Du, Q.; Zhang, Y.; Li, B.; Ke, C.; Ye, Y.; Du, Q. *J. Chromatogr. A* **2013**, *1271*, 67.
4. Edelmann, M.; Kariluoto, S.; Nystrom, L.; Piironen, V. *Food Chem.* **2012**, *135*, 1938.
5. Wang, H. D.; Xie, R.; Hui N. C.; Song, H.; Yang, M.; Liu, S.; Chu, L. Y. *Chem. Eng. Sci.* **2009**, *64*, 1462.
6. Lofgreen, J. E.; Moudrakovski, I. L.; Ozin, G. A. *ACS Nano* **2011**, *5*, 2277.
7. Yu, D.; Zeng, Y.; Qi, Y.; Zhou, T.; Shi, G. *Biosens. Bioelectron.* **2012**, *38*, 270.
8. Kan, X.; Xing, Z.; Zhu, A.; Zhao, Z.; Xu, G.; Li, C.; Zhou, H. *Sens. Actuators B* **2012**, *168*, 395.
9. Zhang, Z.; Zhang, M.; Liu, Y.; Yang, X.; Luo, L.; Yao, S. *Sep. Purif. Technol.* **2012**, *87*, 142.
10. Ansell, R. J.; Kuah, J. K.; Wang, D.; Jackson, C. E.; Bartle, K. D.; Clifford, A. A. *J. Chromatogr. A* **2012**, *1264*, 117.
11. Ng, S. M.; Narayanaswamy, R. *Sens. Actuators B* **2009**, *139*, 156.
12. Athikomrattanakul, U.; Katterle, M.; Gajovic-Eichelmann, N.; Scheller, F. W. *Talanta* **2011**, *84*, 274.
13. Kirsch, N.; Hedin-Dahlström, J.; Henschel, H.; Whitcombe, M. J.; Wikman, S.; Nicholls, I. A. *J. Mol. Catal. B* **2009**, *58*, 110.
14. Sueyoshi, Y.; Fukushima, C.; Yoshikawa, M. *J. Membr. Sci.* **2010**, *357*, 90.
15. Sergeyeva, T. A.; Gorbach, L. A.; Piletska, E. V.; Piletsky, S. A.; Brovko, O. O.; Honcharova, L. A.; Lutsyk, O. D.; Sergeeva, L. M.; Zinchenko, O. A.; El'skaya, A. V. *Anal. Chim. Acta.* **2013**, *770*, 161.
16. Deng, H.; Gao, L.; Zhang, S.; Yuan, J. *Ind. Eng. Chem. Res.* **2012**, *51*, 14018.
17. Meng, M. J.; Wang, Z. P.; Ma, L. L.; Zhang, M.; Wang, J.; Dai, X. H.; Yan, Y. S. *Ind. Eng. Chem. Res.* **2012**, *51*, 14915.
18. Meng, M. J.; Feng, Y. H.; Zhang, M.; Liu, Y.; Ji, Y. J.; Wang, J.; Wu,Y. L.; Yan, Y. S. *Chem. Eng. J.* **2013**, *225*, 331.
19. Zhao, Y. Y.; Ma, Y. X.; Li, H.; Wang, L. Y. *Anal. Chem.* **2012**, *84*, 386.
20. Yang, H. H.; Zhang, S. Q.; Yang, W.; Chen, X. L.; Zhuang, Z. X.; Xu, J. G.; Wang, X. R. *J. Am. Chem. Soc.* **2004**, *126*, 4054.
21. Ke, X. B.; Zhu, H. Y.; Gao, X. P.; Liu, J. W.; Zheng, Z. F.; *Adv. Mater.* **2007**, *19*, 785.
22. Popat, K. C.; Mor, G.; Grimes, C. A.; Desai, T. A. *Langmuir* **2004**, *20*, 8035.
23. Han, J.; Wang, Y.; Liu, Y.; Li, Y. F.; Lu, Y.; Yan, Y. S.; Ni, L. *Anal. Bioanal. Chem.* **2013**, *405*, 1245.
24. Ulbricht, M. *J. Chromatogr. B* **2004**, *804*, 113.
25. Ferreira, S. L. C.; Bruns, R. E.; Ferreira, H. S.; Matos, G. D.; David, J. M.; Brandao, G. C.; da Silva, E.G. P.; Portugal, L. A.; dos Reis, P. S.; Souza, A. S. *Anal. Chim. Acta.* **2007**, *597*, 179.